Brief Communication

Structural Basis of Cooperative Ligand Binding by the Glycine Riboswitch

Ethan B. Butler,[1] Yong Xiong,[1] Jimin Wang,[1] and Scott A. Strobel[1,*]
[1]Department of Molecular Biophysics and Biochemistry, Yale University, New Haven, CT 06520-8114, USA
*Correspondence: scott.strobel@yale.edu
DOI 10.1016/j.chembiol.2011.01.013

SUMMARY

The glycine riboswitch regulates gene expression through the cooperative recognition of its amino acid ligand by a tandem pair of aptamers. A 3.6 Å crystal structure of the tandem riboswitch from the glycine permease operon of *Fusobacterium nucleatum* reveals the glycine binding sites and an extensive network of interactions, largely mediated by asymmetric A-minor contacts, that serve to communicate ligand binding status between the aptamers. These interactions provide a structural basis for how the glycine riboswitch cooperatively regulates gene expression.

INTRODUCTION

Cooperative ligand binding, as exemplified by oxygen binding to hemoglobin, is typically thought to be the exclusive domain of proteins, but the discovery of the glycine riboswitch demonstrated that cooperative ligand binding also plays a role in RNA-based systems (Barrick et al., 2004; Mandal et al., 2004). Riboswitches effect genetic control through the recognition of a specific small molecule ligand and are typically found in the untranslated regions of mRNAs (Nudler and Mironov, 2004). Although some riboswitches make use of multiple domains to attenuate gene expression in response to changes in the concentration of one or more ligands, the tandem-aptamer glycine riboswitch is unique in that its two aptamers, or ligand binding domains, each recognize glycine and binding is cooperative (Figure 1A) (Lee et al., 2010; Mandal et al., 2004; Sudarsan et al., 2006; Welz and Breaker, 2007). The RNA acts as a transcriptional "on" switch to increase the expression of glycine transport and cleavage genes as concentrations of glycine increase, allowing greater flexibility for carbon metabolism in the host organism (Mandal et al., 2004). The ability to bind cooperatively allows the glycine riboswitch to transition from a fully off-state to a fully on-state across a narrow concentration gradient, improving the sensitivity of gene regulation (Kwon and Strobel, 2008; Mandal et al., 2004).

The glycine riboswitch is composed of two similar but nonidentical aptamers connected by a flexible tether. Each aptamer contains three helical segments (P1, P2, and P3) that converge around a central loop (Figure 1A). Helices P1 and P3 and the joining segments J1/2 and J3/1 show high levels of sequence conservation, while the sequence and helix length of

P2 are not conserved (Barrick et al., 2004; Mandal et al., 2004). Residues within P3, particularly the adenosines in the P3a bulge, and the purines in the central loop (J1/2 and J3/1) become more structured upon glycine binding (Kwon and Strobel, 2008; Mandal et al., 2004). Biochemical studies suggested that a tertiary contact necessary for cooperativity between the aptamers occurs between P3 of the second aptamer (Apt2) and P1 of the first (Apt1) (Erion and Strobel, 2011; Kwon and Strobel, 2008). These tertiary contacts form as a part of large conformational rearrangements that cause compaction in the RNA (Erion and Strobel, 2011; Kwon and Strobel, 2008; Lipfert et al., 2007). In order to understand the structural basis of cooperative ligand binding in an RNA system, we determined the crystal structure (3.6 Å resolution) of the tandem-aptamer glycine riboswitch from the glycine permease operon (FN0328) of *Fusobacterium nucleatum* (Figures 1B and 1C and Table 1; see Figure S1 available online).

RESULTS AND DISCUSSION

Global description of the Riboswitch Structure

Based on the crystal structure, both aptamers adopt a similar y-shaped structure and interact to create a pseudosymmetric dimer (Figure 1). Within an individual aptamer the three helices are coplanar (Figures 1D and 1E). Helices P2 and P3 stack to form an extended helix, and the third helix, P1, branches away from P2-P3 at an angle of 50° relative to helix P3. Several of the purine nucleotides in the central loop are unpaired but they form a continuous chain of stacked residues with P1. The two aptamers "dimerize" by packing the P1 helix of one aptamer against the P3 helix of the other resulting in a tertiary structural fold that is three helices thick. The P1 helices from both aptamers are adjacent and parallel to each other in the middle of the fold, sandwiched on both sides by a P2-P3 helix (Figures 1B and 1C).

Ligand Recognition and Binding Pocket Structure of the Glycine Riboswitch

The riboswitch binds two molecules of glycine, one to each aptamer (Figure 2). In both cases, the asymmetric A-rich bulge between helices P3 and P3a forms the amino acid binding pocket. Modification to nucleotides in P3a showed strong and symmetrical interference effects consistent with an important role in ligand binding (Kwon and Strobel, 2008). The two binding sites are close together in three-dimensional space, with the glycines less than 25 Å apart. A key feature of each binding site is U50 (Apt1 numbering), a universally conserved residue predicted to form a wobble pair with the opposing G (G38) in
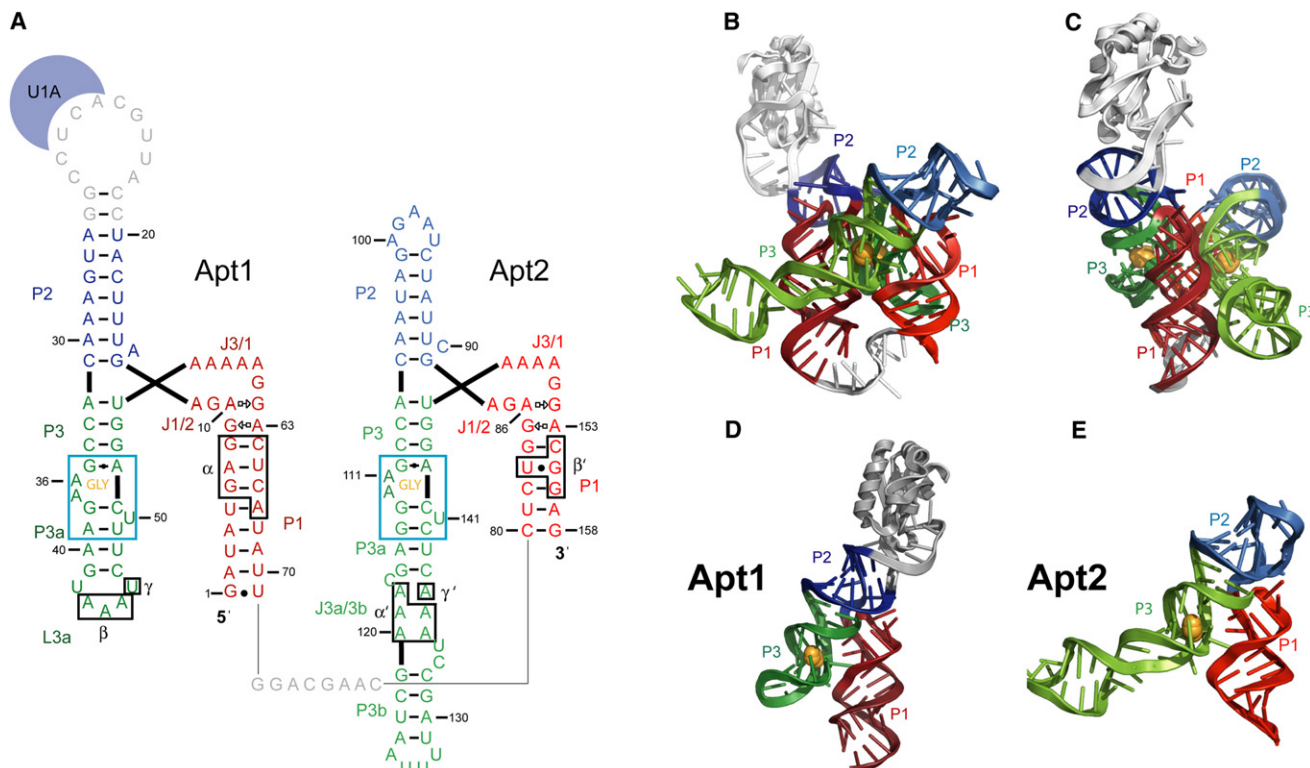
Figure 1. Structure of the Glycine Riboswitch Tandem Aptamer Domain

(A) Secondary structure representation of the crystallized glycine aptamers. Helices P1, P2, and P3 are colored red, blue, and green, respectively. Glycine is shown in orange and residues that form the glycine binding pocket are boxed. The U1A protein, U1A binding loop, and linker region are shown in gray. Numbering is the same as was previously used for this sequence (Kwon and Strobel, 2008). Watson-Crick base pairs are denoted by dashes. Other base pairs are indicated using standard nomenclature (Leontis and Westhof, 2001). Tertiary contacts between the aptamers are boxed and labeled α/α', β/β', and γ/γ'.

(B) Crystal structure of the *F. nucleatum* glycine riboswitch aptamer domain. Coloring is the same as used in (A).

(C) 90° rotation of (B).

(D and E) Structures of the single aptamer domains, Apt1 (D) and Apt2 (E). See also Figure S1. Coloring is the same as in (A).

helix P3a. Instead, G38 pairs with C51, and U50 presents its Watson-Crick face to hydrogen bond with the amino acid (Figure 2A). The entrance to the glycine binding site is framed by the phosphate backbone of residues G35, A36, A37, G38, U46, and C47. The close approach of these phosphates is stabilized by a pair of metals (M1 and M2) that allow the base of A36 to flip out of the binding pocket and into the central loop where it mediates a cross-strand stack near the top of the P1 helix (Figure 2B; Figure S2A). Displacement of A36 creates a pocket into which glycine can bind and is likely to be a key element in cooperativity (see below).

We observe clear density for glycine, but the symmetrical character of the ligand and relatively low resolution of the structure are insufficient to unambiguously orient the amino acid within the binding pocket. One chemically plausible orientation consistent with the electron density has the carbonyl of glycine coordinated to M2 and the N3 of U50, while the amine hydrogen bonds with the O2 carbonyl group of U50 and the O6 carbonyl of G38 (Figure 2B). In this orientation, the α-carbon of the amino acid makes Van der Waals contact with the major groove functional groups of the U49:A39 base pair, which may explain how the riboswitch is able to distinguish glycine from alanine and all other amino acids with a side chain. There is sufficient space

near the carboxylic acid group to accommodate the glycine methyl ester, one of the few glycine derivatives that retain some affinity for the RNA (Mandal et al., 2004). Alternatively the glycine may occupy the reverse orientation with its carbonyl coordinated to M1 and the amino group hydrogen-bonded with the O2 of U50 (Figure S2B). The first model is a better fit to the binding geometry and electron density, but in both models U50 and metal ions play a prominent role in glycine recognition.

Sites of Interaction between Aptamers

The global structure of the tandem aptamer reveals the interaptamer contacts that play a role in cooperative ligand binding. These are predominantly pseudodyad symmetric interactions between the P1 region of one aptamer and the P3 stem of the other. There are three sets of interactions that comprise the interaptamer contacts, which we have termed α, β, and γ (Figures 1A and 3).

The α interaction is the most extensive of the interaptamer contacts. It forms between the top three base pairs of P1 in Apt1 and the Apt2 A-rich bulge between P3a and P3b (J3a/3b), just three base pairs from the glycine binding site. Five adenosines, two from one side (A135 and A136) and three from the other side (A118–A120) of the J3a/3b asymmetric loop, create

Table 1. Data Collection and Refinement Statistics

	Native	0.5 mM iridium Hexamine		
		Inflection	Remote	Peak
Data Collection				
Space group	$P2_12_12_1$	$P2_12_12_1$	$P2_12_12_1$	$P2_12_12_1$
Cell dimensions				
a, b, c (Å)	54.6, 104.6, 156.5	53.5, 98.7, 154.5	53.4, 98.4, 154.1	52.7, 97.5, 154.4
α, β, γ (°)	90.0, 90.0, 90.0	90.0, 90.0, 90.0	90.0, 90.0, 90.0	90.0, 90.0, 90.0
Wavelength	1.079	1.1054	1.08	1.1050
Resolution (Å)	3.6 (3.73–3.60)[a]	3.85 (3.99–3.85)	3.6 (3.73–3.6)	4.1 (4.25–4.1)
R_{merge}	0.108 (>1.0)	0.06 (0.847)	0.055 (0.745)	0.108 (0.906)
$I/\sigma I$	19.5 (1.76)	16.2 (1.45)	17.0 (0.98)	12.1 (0.93)
Completeness (%)	99.8 (99.9)	94.5 (83.3)	95.3 (78.3)	99.0 (96.7)
Redundancy	13.5 (11.9)	2.4 (2.8)	2.4 (3.0)	3.7 (2.8)
Phasing				
Figure of Merit	0.35 (MAD); 0.57 (after density modification)			
Refinement				
Resolution (Å)	25–3.6			
No. reflections	10,796			
R_{work}/R_{free}	28.2/31.0			
No. atoms				
Protein	749			
RNA	3624			
Ligand/ion	23			
Water	20			
B-factors				
Protein	169			
RNA	200			
Ligand/ion	154			
Water	116			
Rmsds				
Bond lengths (Å)	0.013			
Bond angles (°)	1.32			

[a] Values in parenthesis are for highest resolution shell.

a continuous base stack and form five consecutive A-minor interactions with the minor groove edge of P1 (Figure 3A and 3B) (Nissen et al., 2001). The first and third base pairs of the P1 helix (G8-C64 and G6-C66) each form a type I A-minor interaction (with A136 and A119, respectively) (Figure 3B), while the second base pair (A7-U65) forms two type II A-minor contacts (A135 and A118), one on each strand of the helix (Figure 3B). Even the fourth base pair (U5-A67) is contacted, albeit less extensively by a type 0 A-minor interaction with A120 (Figure 3B). A number of these interactions explain previous biochemical observations, such as the critical role of the 2'-OHs of A7, A118, and A135 for riboswitch function (Kwon and Strobel, 2008). Consistent with the role of these interactions in cooperative ligand binding, mutation of the third base pair of P1 (a C-G base pair) to a U·G in the *Vibrio cholerae* glycine riboswitch of the VC1422 gene resulted in loss of cooperativity, presumably by disrupting the formation of the type I A-minor interaction (Kwon and Strobel, 2008).

The β interaction is thematically similar but less extensive than the contacts made in α. This tertiary contact involves the matching regions of the two aptamers, namely Apt1 adenosines in the L3a loop and the P1 stem of Apt2 (Figure 3C). Like α, the β interaction is within a few base pairs of a glycine binding site, but in this case only three base pairs of Apt2 P1 are contacted (Figure S3). As in α, the first base pair in P1 (G84-C154) is recognized by a type I A-minor interaction (with A45), but the second base pair (U83-G155) is contacted by just a single type II interaction (G155 with A44). The difference between the α and β contacts are even more evident at the third base pair (C82-G156) which instead of forming an extensive type I contact, makes a single hydrogen bond to A43, and no contacts are made to the fourth base pair. The extent of the β interaction appears to be limited by the geometry of the Apt1 adenosines, which are constrained by the sharp hairpin turn of L3a. The smaller interface of the β relative to the α interaction is consistent with NAIM and biochemical results which showed that the third base pair of
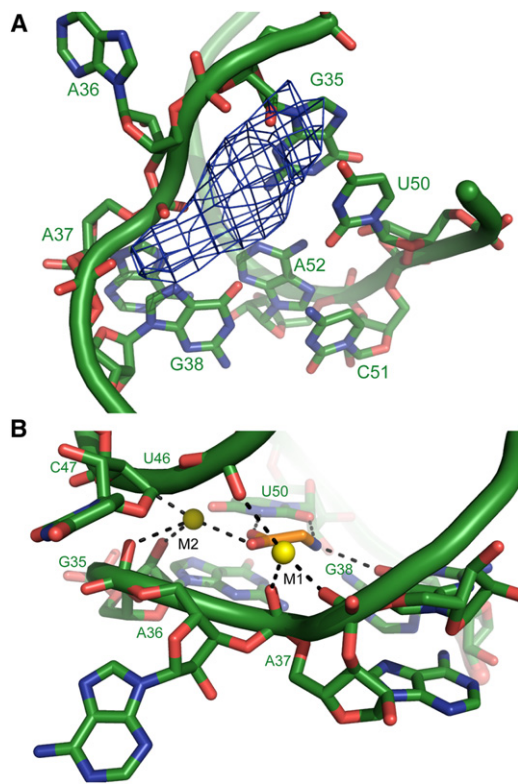
Figure 2. Glycine Binding Pocket
(A) Glycine binding pocket in Apt1. Coloring is the same as in (Figure 1A). F_o-F_c maps generated from a model lacking glycine and metals is shown in blue (contoured at 2.8σ). Universally conserved U50 presents its Watson-Crick face to the binding pocket, while A36 is flipped out to create a cavity for glycine binding.
(B) Glycine binding pocket metals M1 and M2 (shown in yellow). See also Figure S2.

P1 in Apt1 was critical for cooperativity, but minor groove chemical modifications and even a wobble pair were fully tolerated at the third base pair of Apt2 (Kwon and Strobel, 2008).

A third interaptamer contact (γ) is positioned such that it may play an important role in communicating the status of ligand binding between the two binding pockets. The γ interaction forms between U46 in Apt1 and A137 in Apt2 (Figure 3D). A137 flips out of the helical stack and adopts a syn conformation which allows it to make a Hoogsteen base pair with U46. These two nucleotides are flanked on the 5′ end by the adenosines that form the α and β interfaces and flanked on the 3′ end by nucleotides that form the glycine binding pocket. While the particular nucleotides are not highly conserved, multiple sequence alignments indicate that when one nucleotide is a U there is a bias toward the interaction partner occurring as an A. The sum of these tertiary interactions results in an RNA that can communicate the ligand binding status from one aptamer to the other (Erion and Strobel, 2011; Kwon and Strobel, 2008; Mandal et al., 2004).

Subsequent to the submission of this paper, the structure of a single aptamer glycine riboswitch was independently reported by Huang et al. (2010) at 2.85 Å resolution. It is noteworthy that the major features of an isolated aptamer, including helix orientation, nucleotide displacement from the binding pocket, and

glycine binding appear to be consistent with that reported for the single aptamer. The core region of each structure superposes well, with an average displacement of just 0.92 Å and the glycine orientation depicted in Figure 2B matches that reported by Huang et al. Although their structure is of an isolated single aptamer, the RNA forms a homodimer within the crystal's asymmetric unit. Based upon the interaptamer contacts made in the crystal, they proposed that A-minor interactions between P1 and P3 are responsible for cooperative ligand binding. Our structure confirms that the A-minor interactions (α, β) present in their crystal contacts do occur in a natural tandem glycine riboswitch, and reveals the asymmetric character of these interactions. They also observe interaptamer pi-stacking interactions between the two A65 residues, which are structurally different, but thematically similar to the noncanonical γ interaction between U46 and A137 that is present in this dual aptamer structure.
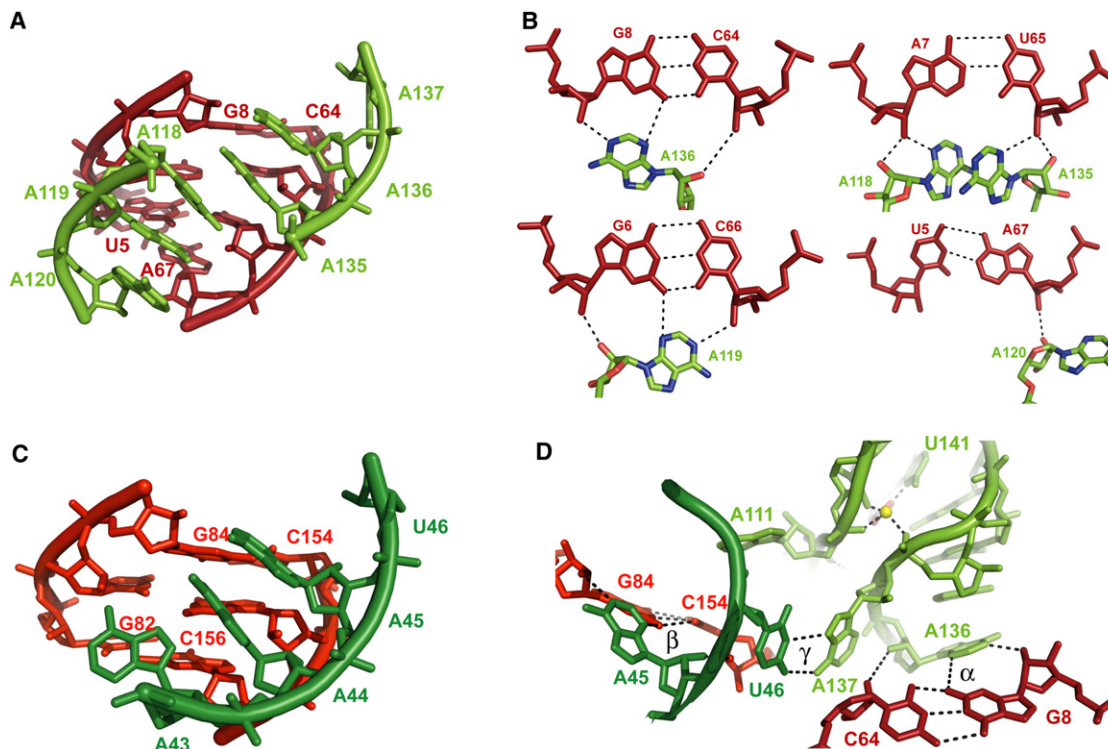
SIGNIFICANCE

This structure in concert with previous biochemical data suggests a mechanism for cooperative ligand binding. The question is how does glycine binding to one aptamer promote glycine binding to the second? In hemoglobin, the classic model for cooperative ligand binding, structural changes between subunits are triggered by ligand binding at one site resulting in a transition from the low affinity (T) to high affinity (R) state (Ackers et al., 1992; Royer et al., 2001; Turner et al., 1992). Many of the fundamental elements observed in hemoglobin cooperativity are consistent with structural features of cooperative glycine binding to this RNA (Perutz, 1970). The J1/3, J3/1, and P1 regions become more structured with the addition of glycine, likely due to a series of stacking interactions that can only form when A36 or A111 are displaced from the binding pocket (Kwon and Strobel, 2008; Mandal et al., 2004). Stabilization of the P1 region enhances formation of interaptamer contacts α or β, which have been shown to play a role in cooperativity (Erion and Strobel, 2011; Kwon and Strobel, 2008). Our structure reveals the close proximity of all the interaptamer contacts to the two binding pockets (α and β are within 11 Å of glycine, γ is within 8 Å), which suggests that structural rearrangements induced by glycine binding in one pocket are translated into conformational changes that enhance ligand binding in the other pocket through these interfaces. In the case of both hemoglobin and the glycine riboswitch, structural rearrangements induced when the first ligand is bound trigger changes in interdomain contacts that stabilize a state more competent to bind a second ligand.

EXPERIMENTAL PROCEDURES

Crystallization, Data Collection, and Refinement

Figure 3. Interaptamer Interactions Leading to Cooperative Ligand Binding
(A) Global view of cooperative interface α, Apt1 P1 shown in dark red and Apt2 J3a/3b shown in light green.
(B) A-minor motif interactions that compose the α cooperative interface. See also Figure S3.
(C) Global view of interface β, Apt1 L3a shown in dark green and Apt2 P1 shown in red.
(D) Global view of interface γ. Coloring is the same as in (1A). Nucleotides in γ lie directly between cooperative interfaces α or β and the ligand binding pocket.

(Otwinowski and Minor, 1997). Eleven Ir atom sites were located in SHELXD using a two wavelength MAD data set as well as a SAD data set (peak) collected at a different position of the same crystal (Sheldrick, 2008; Terwilliger and Berendzen, 1999). Initial maps were improved by multidomain multicrystal averaging in DMMulti using the native data set, the nonisomorphous iridium soak data set (R_{iso} = 57%), a native data set, and the U1A region from the hairpin ribozyme data set (3HHN) (Cowtan and Main, 1996; Potterton et al., 2002). The resulting maps were of sufficient quality to build an initial model, which was refined in Refmac v.5.5.0110 (Murshudov et al., 1997). Model building was done in Coot with the aid of the B-factor sharpening function (Emsley et al., 2010). Electron density attributed to be the ligand was relatively weak using calculated model phases. To improve this, the binding pocket density was averaged between the two aptamers in both the native and iridium data sets, resulting in significant improvement in density for Apt1 (Cowtan and Main, 1996; Potterton et al., 2002).

ACCESSION NUMBERS

Coordinates and structure factors for the glycine riboswitch are available in the Protein Data Bank (http://www.rcsb.org/) under ID code 3P49.

SUPPLEMENTAL INFORMATION

Supplemental Information includes three figures and can be found with this article online at doi:10.1016/j.chembiol.2011.01.013.

REFERENCES

Ackers, G.K., Doyle, M.L., Myers, D., and Daugherty, M.A. (1992). Molecular code for cooperativity in hemoglobin. Science *255*, 54–63.

Barrick, J.E., Corbino, K.A., Winkler, W.C., Nahvi, A., Mandal, M., Collins, J., Lee, M., Roth, A., Sudarsan, N., Jona, I., et al. (2004). New RNA motifs suggest an expanded scope for riboswitches in bacterial genetic control. Proc. Natl. Acad. Sci. USA *101*, 6421–6426.

Cowtan, K.D., and Main, P. (1996). Phase combination and cross validation in iterated density-modification calculations. Acta Crystallogr. D Biol. Crystallogr. *52*, 43–48.

Emsley, P., Lohkamp, B., Scott, W.G., and Cowtan, K. (2010). Features and development of Coot. Acta Crystallogr. D Biol. Crystallogr. *66*, 486–501.

Erion, T.V., and Strobel, S.A. (2011). Identification of a tertiary interaction important for cooperative ligand binding by the glycine riboswitch. RNA *17*, 74–84.

Huang, L., Serganov, A., and Patel, D.J. (2010). Structural insights into ligand recognition by a sensing domain of the cooperative glycine riboswitch. Mol. Cell *40*, 774–786.

Kwon, M., and Strobel, S.A. (2008). Chemical basis of glycine riboswitch cooperativity. RNA *14*, 25–34.

Lee, E.R., Baker, J.L., Weinberg, Z., Sudarsan, N., and Breaker, R.R. (2010). An allosteric self-splicing ribozyme triggered by a bacterial second messenger. Science *329*, 845–848.

Leontis, N.B., and Westhof, E. (2001). Geometric nomenclature and classification of RNA base pairs. RNA *7*, 499–512.

Lipfert, J., Das, R., Chu, V.B., Kudaravalli, M., Boyd, N., Herschlag, D., and Doniach, S. (2007). Structural transitions and thermodynamics of a glycine-dependent riboswitch from *Vibrio cholerae*. J. Mol. Biol. *365*, 1393–1406.

Mandal, M., Lee, M., Barrick, J.E., Weinberg, Z., Emilsson, G.M., Ruzzo, W.L., and Breaker, R.R. (2004). A glycine-dependent riboswitch that uses cooperative binding to control gene expression. Science *306*, 275–279.

Murshudov, G.N., Vagin, A.A., and Dodson, E.J. (1997). Refinement of macromolecular structures by the maximum-likelihood method. Acta Crystallogr. D Biol. Crystallogr. *53*, 240–255.

Nissen, P., Ippolito, J.A., Ban, N., Moore, P.B., and Steitz, T.A. (2001). RNA tertiary interactions in the large ribosomal subunit: the A-minor motif. Proc. Natl. Acad. Sci. USA *98*, 4899–4903.

Nudler, E., and Mironov, A.S. (2004). The riboswitch control of bacterial metabolism. Trends Biochem. Sci. *29*, 11–17.

Otwinowski, Z., and Minor, W. (1997). Processing of X-ray diffraction data collected in oscillation mode. Methods Enzymol. *276*, 307–326.

Perutz, M.F. (1970). Stereochemistry of cooperative effects in haemoglobin. Nature *228*, 726–739.

Potterton, E., McNicholas, S., Krissinel, E., Cowtan, K., and Noble, M. (2002). The CCP4 molecular-graphics project. Acta Crystallogr. D Biol. Crystallogr. *58*, 1955–1957.

Royer, W.E., Jr., Knapp, J.E., Strand, K., and Heaslet, H.A. (2001). Cooperative hemoglobins: conserved fold, diverse quaternary assemblies and allosteric mechanisms. Trends Biochem. Sci. *26*, 297–304.

Sheldrick, G.M. (2008). A short history of SHELX. Acta Crystallogr. A *64*, 112–122.

Sudarsan, N., Hammond, M.C., Block, K.F., Welz, R., Barrick, J.E., Roth, A., and Breaker, R.R. (2006). Tandem riboswitch architectures exhibit complex gene control functions. Science *314*, 300–304.

Terwilliger, T.C., and Berendzen, J. (1999). Automated MAD and MIR structure solution. Acta Crystallogr. D Biol. Crystallogr. *55*, 849–861.

Turner, G.J., Galacteros, F., Doyle, M.L., Hedlund, B., Pettigrew, D.W., Turner, B.W., Smith, F.R., Moo-Penn, W., Rucknagel, D.L., and Ackers, G.K. (1992). Mutagenic dissection of hemoglobin cooperativity: effects of amino acid alteration on subunit assembly of oxy and deoxy tetramers. Proteins *14*, 333–350.

Welz, R., and Breaker, R.R. (2007). Ligand binding and gene control characteristics of tandem riboswitches in *Bacillus anthracis*. RNA *13*, 573–582.